AGU100 ADVANCING EARTH AND SPACE SCIENCE

Geophysical Research Letters

RESEARCH LETTER
10.1029/2018GL078799

Key Points:
- High compositional viscosity stabilizes thermochemical piles at the core-mantle boundary
- We identify a trade-off between density and viscosity contrast to maintain pile stability
- Pile stability during periods of strong deformation-induced entrainment, for example, pile formation, requires higher viscosity and/or density

Supporting Information:
- Supporting Information S1
- Figure S1
- Figure S2

Correspondence to:
B. H. Heyn,
b.h.heyn@geo.uio.no

Citation:
Heyn, B. H., Conrad, C. P., & Trønnes, R. G. (2018). Stabilizing effect of compositional viscosity contrasts on thermochemical piles. *Geophysical Research Letters*, *45*, 7523–7532. https://doi.org/10.1029/2018GL078799

Received 16 MAY 2018
Accepted 14 JUN 2018
Accepted article online 21 JUN 2018
Published online 14 AUG 2018

Stabilizing Effect of Compositional Viscosity Contrasts on Thermochemical Piles

Björn H. Heyn[1], **Clinton P. Conrad**[1], **and Reidar G. Trønnes**[1,2]

[1]Centre for Earth Evolution and Dynamics, University of Oslo, Oslo, Norway, [2]Natural History Museum, University of Oslo, Oslo, Norway

Abstract The large low shear velocity provinces observed in the lowermost mantle are widely accepted as chemically distinct thermochemical "piles," but their origin and long-term evolution remain poorly understood. The survival time and shape of the large low shear velocity provinces are thought to be mainly controlled by their compositional density, while their viscosity has been considered less important. Based on recent constraints on chemical reactions between mantle and core, a more complex viscosity structure of the lowermost mantle, possibly including high viscosity thermochemical pile material, seems reasonable. In this study, we use numerical models to identify a trade-off between compositional viscosity and density contrasts required for long-term stability of thermochemical piles, which permits lower-density and higher-viscosity piles. Moreover, our results indicate more restrictive stability conditions during periods of strong deformation-induced entrainment, for example, during initial pile formation, which suggests long-term pile survival.

Plain Language Summary Seismic images of the Earth's mantle show two anomalous continent-sized regions close to the core-mantle boundary. The inferred properties of these regions suggest that they have a different composition than the surrounding mantle. Two possible candidate materials have been proposed: accumulated oceanic crust from the Earth's surface or an iron-rich residue remaining from Earth's original magma ocean. Although both materials are denser than the surrounding mantle, it remains unclear whether piles of these chemical heterogeneities can survive at the core-mantle boundary beneath vigorous mantle convection. Numerical models show that the excess density required to preserve these structures is typically larger than indicated by seismological and gravitational observations. In this study, we show that the excess density used in numerical models can be reduced toward the observed values if the pile material is also stiffer than the surrounding mantle. Furthermore, we show that piles must be denser and/or stiffer to avoid destruction during episodes of strong deformation. Because pile formation probably includes vigorous deformation, we expect long-term survival of the piles after their formation is completed.

1. Introduction

The presence of a dominant degree-2 structure of low seismic velocities in the lowermost mantle has been revealed by seismic tomography models throughout the last decades, (e.g., Dziewonski et al., 2010; Garnero et al., 2016; Hager et al., 1985). Although all tomographic models agree on the position of the so-called large low shear velocity provinces (LLSVPs; Dziewonski et al., 2010; Garnero & McNamara, 2008; Garnero et al., 2016) beneath Africa and the Pacific (Cottar & Lekic, 2016; Garnero & McNamara, 2008; Lekic et al., 2012), their origin and evolution with time is still under debate. While some studies suggest a purely thermal origin of the observed structures (e.g., Davies et al., 2012; Schuberth, Bunge, & Ritsema, 2009; Schuberth, Bunge, Steinle-Neumann et al., 2009; Schuberth et al., 2012) or indicate a dominant effect of temperature (Simmons et al., 2009), most geodynamic models involve a compositionally distinct and dense pile material (e.g., Li, Deschamps, et al., 2014, 2015; McNamara & Zhong, 2004, 2005; Mulyukova et al., 2015; Nakagawa & Tackley, 2011; Tackley, 2012). Typical arguments supporting chemical piles include their sharp boundaries (see review by Garnero et al., 2016), although they might also be explained by strong temperature gradients (Davies et al., 2012; Schuberth, Bunge, Steinle-Neumann et al., 2009; Schuberth et al., 2012).

Two different possible candidate materials for chemical LLSVPs, recycled oceanic crust (mid-ocean ridge basalt [MORB]; Li & McNamara, 2013; Li, McNamara, et al., 2014; Mulyukova et al., 2015; Nakagawa & Tackley, 2011), or primordial iron-rich cumulates (Li, Deschamps, et al., 2014, 2015; McNamara & Zhong, 2004, 2005; Nakagawa & Tackley, 2011) imply different pile formation histories. While MORB would accumulate over time to form the observed structures (Li & McNamara, 2013; Mulyukova et al., 2015), primordial material would start as a layer at the core-mantle boundary (CMB) after crystallization of the magma ocean (Labrosse et al., 2007) and subsequently be deformed by mantle convection to form two antipodal piles (e.g., Li, Deschamps, et al., 2014; Li et al., 2015; McNamara & Zhong, 2004). In both cases, composition may affect the viscosity, which considerably widens the range of possible viscosities in the pile (Torsvik et al., 2016).

Apart from the composition of the piles, their evolution is still under debate. Stability of piles can refer to the evolution of their spatial distribution within the mantle or their survival time. Since we observe these structures 4.5 Gyr after Earth's formation, temporal stability (survival) has to be fulfilled. However, constraints for spatial stability are not as obvious. For at least the last 300 Myr, stability of the current degree-2 structure of LLSVPs has been inferred by Torsvik et al. (2010, 2014, 2016) based on reconstructions of large igneous provinces and kimberlites, which are both related to plumes rising at the LLSVP margins. Additionally, Conrad et al. (2013) showed persistent tectonic divergence above the two LLSVPs for at least the last 250 Myr, suggesting stable upwellings there. Here we consider the conditions necessary to maintain temporal stability of the piles under the simplifying assumption of spatial stability of mantle flow and surface tectonics, which gives us the minimum requirements of pile survival.

Survival of thermochemical piles at the CMB is thought to be mostly controlled by the chemical density contrast between the pile and the surrounding mantle (e.g., Tackley, 2012). Li, Deschamps, et al. (2014) showed that large temperature-induced viscosity contrasts (factor of 10^6) help to stabilize piles, while comparably small compositional viscosity contrasts ($\leq$100 times) are less important for strongly temperature-controlled viscosity profiles. However, a higher intrinsic pile viscosity may be required for material with high bulk modulus (Bower et al., 2013). Laboratory experiments of Davaille et al. (2002) also indicate the importance of higher viscosity to reduce entrainment of the dense component. Reactions between the core and a thermally insulated and long-lived basal magma ocean (Labrosse et al., 2007) may provide late-stage bridgmanitic residues with high viscosity and elevated Fe/Mg ratio and density. Since the core is undersaturated in oxygen and oversaturated in silica (Frost et al., 2010; Hirose et al., 2017), SiO_2 from the core would be exchanged with FeO from the basal magma ocean, increasing the bridgmanite-to-ferropericlase ratio and thus the viscosity of the solid material. Another possible origin of dense material could be an overturn by diapiric sinking of Fe-rich cumulates from the upper magma ocean, with subsequent melting and reequilibration with the host rock (Ballmer et al., 2017; Lee et al., 2010). Fe-enriched bridgmanite has also been identified as a reasonable material to explain the anticorrelation of bulk sound and shear wave velocity, while basalt does not reproduce the observations (Deschamps et al., 2012).

Constraints on the temperature dependence of viscosity in the lowermost mantle are limited. Most numerical models assume large thermal viscosity contrasts (e.g., Li, Deschamps, et al., 2014), although geoid constraints argue for a weak temperature dependence (e.g., Yang & Gurnis, 2016). In contrast, the overall density of the LLSVPs has been estimated by Koelemeijer et al. (2017) and Lau et al. (2017), who argue for a neutral buoyancy of the LLSVP volume or a small excess density of about 0.5–1% in the lower part of the LLSVPs, respectively. This also agrees with geoid observations indicating that the upwelling material above the LLSVPs has to overcompensate dense material at the CMB to produce a geoid high (e.g., Liu & Zhong, 2015). However, these measured densities are smaller than those typically required for stability in numerical models of thermochemical convection, even when accounting for both chemical density and thermal expansion. In this work, we will show that a compositionally dependent viscosity can strongly increase the temporal stability of thermochemical piles for smaller excess densities and lower temperature dependence of viscosity compared to previous work.

2. Model Setup

Our numerical models are run in 2-D spherical geometry using the finite element code CitcomS (Tan et al., 2006; Zhong et al., 2000). Conservation equations of mass, energy, and momentum are solved using

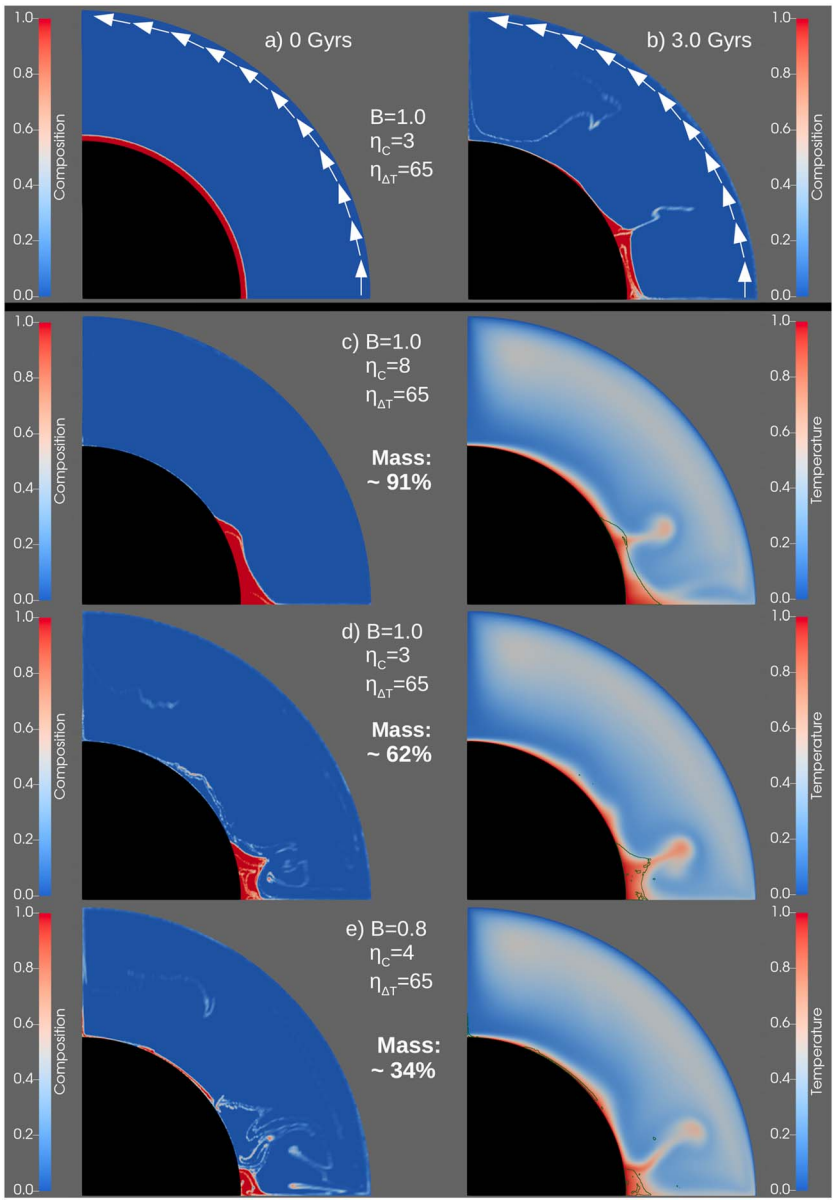

Figure 1. (a) Initial condition and (b) snapshot after 3.0 Gyr show composition for models that start with a dense layer and assume $B = 1.0$, $\eta_{\Delta T} = 65$, and $\eta_C = 3$, showing deformation and increased entrainment during the transition from a layer to a pile. White arrows indicate imposed plate velocity. Examples of the (left) composition and (right) temperature of piles with remaining mass of (c) 91%, (d) 62%, and (e) 34% after 4.5 Gyr and the parameter combinations used to produce them. Dark lines in the temperature fields indicate the pile shapes for $cl = 0.8$.

the Boussinesq approximation. Parameters described below are given in nondimensional form and are listed in the supporting information (Table S1). The Rayleigh number describes the vigor of convection and is set to 10^7. The domain is a quarter of an annulus chosen along the equator with a grid of 313 by 91 nodes in longitude and depth, respectively. The mesh is refined in the lowermost 809 km, so that the effective resolution at the CMB is 17 km by 17 km. As discussed later, this resolution is not sufficient to capture the entrainment rates precisely but allows for interpretation of time-integrated pile masses relevant for long-term stability. A constant uniform velocity boundary condition of 1.48 cm/year (Figure 1a) is imposed on the surface to force a single-plate degree-2 flow structure, while all other boundaries are free slip. Heat is introduced into the system by basal and moderate internal heating. We track the advection of composition using tracer particles (McNamara & Zhong, 2004), 20 particles per element (a total of ~1.1 million), and the tracer-ratio method

(Tackley & King, 2003) to determine the composition within each element. The density contrast between enriched and regular mantle is defined via the buoyancy ratio

$$B = \frac{\Delta\rho_C}{\alpha\rho\Delta T},$$

where $\Delta\rho_C$ is the density difference due to composition. α, ΔT, and ρ are the thermal expansion coefficient, temperature difference, and density, respectively.

Viscosity depends on temperature, depth, and the composition, given by

$$\begin{aligned}\eta(z,T,C) &= \eta_0(z)\eta_{\Delta T}(z,T)\exp\left[C\ln\eta_C\right]\\ &= \eta_0(z)\exp\left[\frac{E_\eta(z)}{T^* + T_\eta(z)} - \frac{E_\eta(z)}{1+T_\eta(z)} + C\ln\eta_C\right]\end{aligned}$$

with the nondimensional temperature $T^* = \min(\max(T,0),1)$. The depth dependence is implemented as stepwise adjustments of the viscosity prefactor η_0, the activation energy E_η, and the temperature offset T_η (see Table S2). η_C is the viscosity contrast due to composition, and C is the composition value between 0 and 1. The thermal viscosity contrast $\eta_{\Delta T}$ describes the maximum potential viscosity variations due to temperature in the lower mantle and is varied in the range 2.3 to 330, while η_C assumes values between 1 and 20.

Models start with a dense layer at the CMB (see Figure 1a) and are run for at least 4.5 Gyr. We calculate the remaining mass m and volume of the pile for each time step by defining elements as belonging to the pile if their composition is above a contour value of $cl = 0.8$ (>80% pile material) and if they are connected to another pile element below or at the same depth. This algorithm hence accounts for all compositionally distinct patches connected to the CMB and does not discriminate between all material occurring in a single pile or distributed between two or more.

3. Observed Pile Structures

Piles are characterized by the mass remaining after 4.5 Gyr. Piles with about 80% retained mass can be considered stable, while piles with approximately 50% of the original mass are metastable. "Stable" piles with >80% mass remaining are compact and have only small heterogeneities (Figure 1c, $m \sim 91\%$), while almost no dense material is entrained in the mantle. In contrast, both entrainment and internal heterogeneities increase with decreasing compositional viscosity contrast (Figure 1d, $m \sim 62\%$) and density (Figure 1e, $m \sim 34\%$). As a consequence, the mass remaining in the pile is significantly reduced. During the formation of the pile (compare Figure 1b), the dense component is strongly deformed and parts of the material can get ripped off the coherent structure but may later sink back toward the pile.

For pile masses <50%, we observe a range of different structures. All of them are characterized by significant material loss, but pile shapes are considerably affected by the buoyancy ratio and the viscosity contrast. Patches of dense material can get detached from the pile and subsequently be advected with the flow (as seen in Figure 1e). This process is amplified for low buoyancy ratios or in models where mixing between dense components and ambient mantle considerably reduces the initial density contrast. However, an increased viscosity allows patches of dense material to survive one or more mantle overturns before they are completely entrained. Metastable piles (around 50% mass) are in general strongly time dependent and show a pronounced topography and an increased mobility both in lateral and in radial directions.

As can be seen in the temperature field (see Figures 1c–1e, right panel), plumes rise primarily at the edges of the dense piles, as inferred from hotspots, large igneous provinces, and kimberlites (Steinberger & Torsvik, 2012; Torsvik et al., 2014, 2016), although these correlations have been questioned (Austermann et al., 2014; Davies et al., 2015). However, thermal instabilities grow along the CMB and are subsequently pushed toward the pile, where they reshape the edge of the dense material during ascent. Part of the dense component is entrained in the rising plume and may reach the surface. Less buoyant upwellings, consisting of plumes that have lost most of their excess temperature and were pushed on top of the pile, can be seen in Figure 1c (right). This broader upwelling is strongly time dependent and can entrain variable amounts of dense material, which may provide a potential source for heterogeneities observed in magmas of weak hotspots above LLSVPs (e.g., Chauvel et al., 2012).

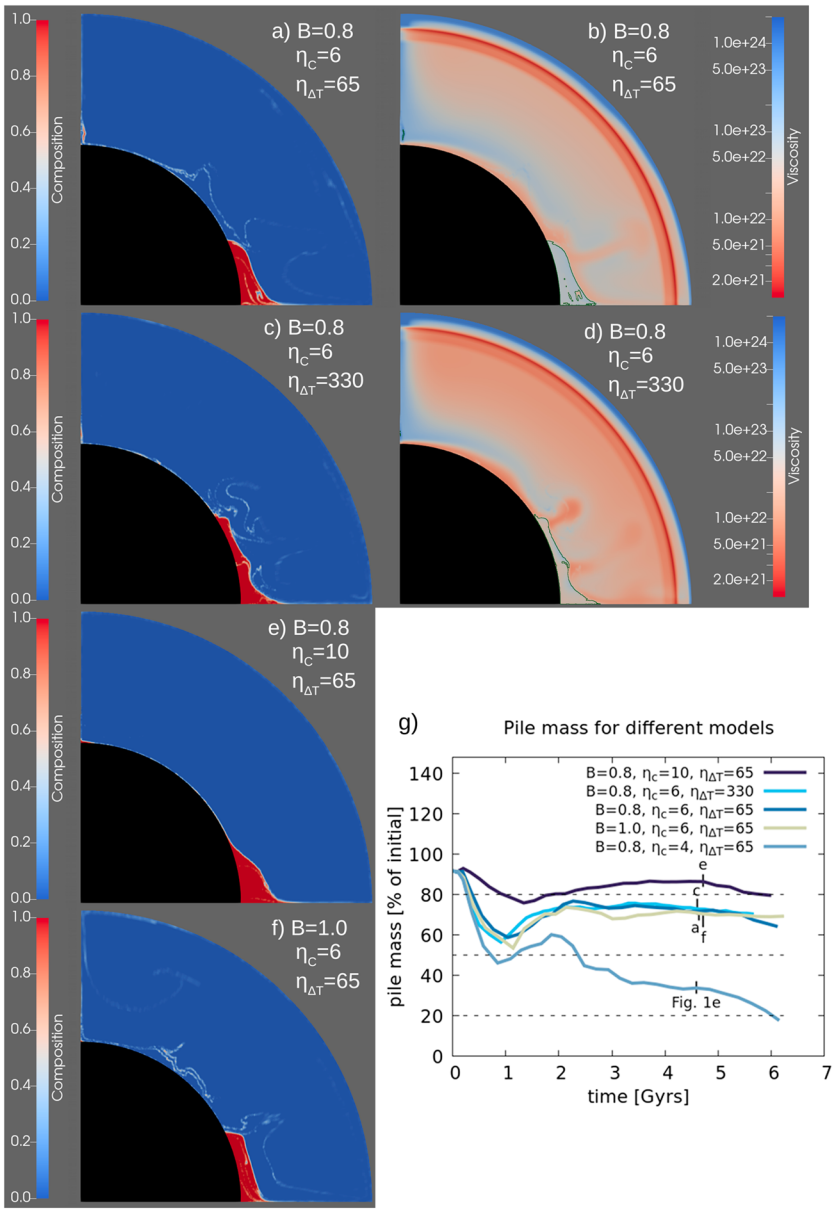

Figure 2. Snapshots of different thermochemical models at 4.5 Gyr. (a) Compositional and (b) viscosity fields for $B = 0.8$, $\eta_{\Delta T} = 65$, $\eta_C = 6$, and for the same parameters except $\eta_{\Delta T} = 330$ (c and d, respectively). Dark lines in the viscosity fields outline the pile shapes for $cl = 0.8$. (e, f) The composition fields for $B = 0.8$, $\eta_{\Delta T} = 65$, $\eta_C = 10$ and $B = 1.0$, $\eta_{\Delta T} = 65$ and $\eta_C = 6$. (g) Temporal evolution of pile masses ($cl = 0.8$) for models discussed in (a)–(f) and Figure 1e.

4. Trade-Off Between Buoyancy Ratio and Viscosity Contrast

For models with a moderate buoyancy number of $B = 0.8$ (excess density of ~2.6% for $\Delta T = 3200$ K, see Table S1), stable piles can be obtained for $\eta_{\Delta T} = 65$ and $\eta_C = 6$ (Figure 2a). However, almost 30% of the initial mass is lost, and the pile exhibits heterogeneities within, indicating that stability may only be temporal. A higher compositional viscosity contrast of $\eta_C = 10$ as for the case in Figure 2e increases the pile mass to about 87% and results in a more homogeneous pile. A similar, though less pronounced effect can be observed for a higher thermal viscosity contrast of $\eta_{\Delta T} = 330$ (Figure 2c). In contrast to η_C, $\eta_{\Delta T}$ causes the pile to flatten instead of doming up (Bower et al., 2013; McNamara & Zhong, 2004) as observed in Figure 2e.

If we increase the buoyancy ratio to $B = 1.0$, the pile mass does not change significantly but the pile contains slightly fewer heterogeneities (Figure 2f). However, the resulting pile structure exhibits a less pronounced topography. A reduction of the buoyancy ratio, or a lower viscosity contract η_C, both result in significantly more

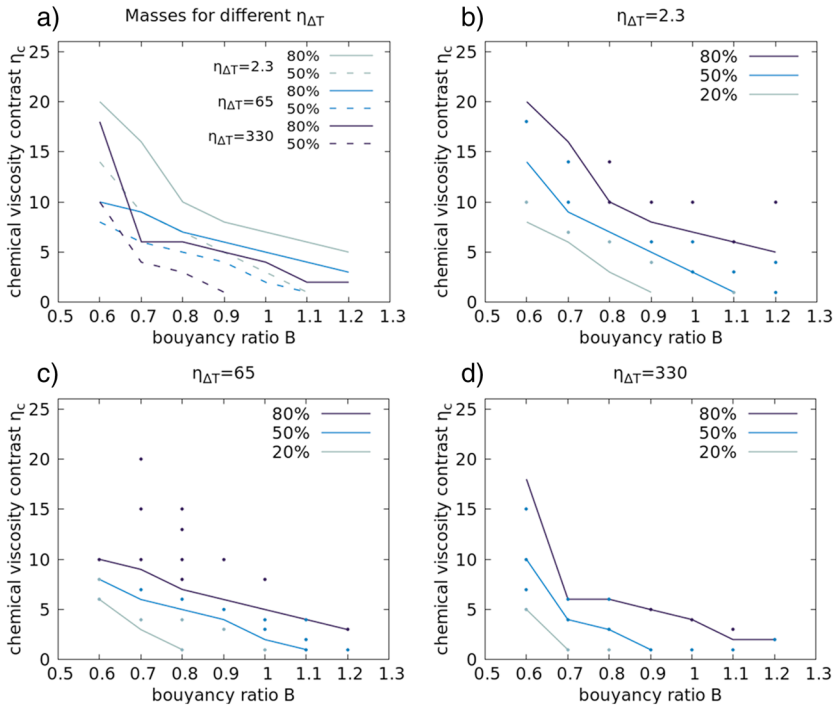

Figure 3. (a) Overview of contour lines for 50% and 80% remaining mass as a function of B, $\eta_{\Delta T}$, and η_C. The observed fields of pile masses with dots indicating the tested parameter combinations for $\eta_{\Delta T} = 2.3$ (b), 65 (c), and 330 (d). Solid lines mark the expected contours of 20%, 50%, and 80% mass remaining.

entrainment of dense material, which agrees with Davaille et al. (2002), and small, highly heterogeneous piles. Between $B = 0.7$ and $B = 1.2$ the chemical viscosity contrast necessary for stability increases with decreasing buoyancy ratio.

The temporal evolution of the pile mass for five models discussed above is shown in Figure 2g. As can be seen, all of them show a more or less pronounced loss of material during the first 1–2 Gyr, while the pile mass slightly recovers afterward for most models. This initial loss is caused by deformation of the starting layer (Figure 1b) that depends on the initial temperature condition (McNamara & Zhong, 2004). During this period, η_C has more importance than B as both the case in Figures 2a and 2f loose the same amount of mass, while the case in Figure 2e does not. After ~1.5 Gyr, when material starts to reaccumulate to the pile, both B and η_C control how much ambient mantle will be included in the dense pile. This determines the effective density and viscosity of the pile and thus its long-term behavior, favoring dense piles for times beyond 6 Gyr.

An overview of contour lines for the remaining mass as a function of buoyancy ratio B, compositional viscosity contrast η_C and thermal viscosity contrast $\eta_{\Delta T}$ (Figure 3a) shows the trade-offs between these parameters. More detailed figures for thermal viscosity contrasts of $\eta_{\Delta T} = 2.3$, 65, and 330, including our tested models as data points (Figures 3b–3d), show that the compositional viscosity contrast necessary for pile stability decreases with increasing buoyancy ratio or increasing thermal viscosity contrast. This trend is consistent for all our models, except for some deviations for $B = 0.6$ (about 1.9% excess density), which marks a lower limit of stability. Models with smaller B (not shown) require significantly higher thermal or chemical viscosity contrasts $\eta_C > 100$ to avoid extensive entrainment of the dense material within 4.5 Gyr. The observation of increased stability with larger $\eta_{\Delta T}$ is consistent with the results of Li, Deschamps, et al. (2014), although we need significantly lower thermal viscosity contrasts when adding even a small compositional viscosity contrast η_C. Our results indicate that the pile does not have to be more viscous than the slab (compare Figures 2b and 2d), but the plume-pile viscosity contrast (controlled by η_C) plays a major role.

5. Stability Conditions for Different Pile Deformation Histories

Little is known about the initial conditions of pile formation. A compositionally layered mantle with a temperature gradient is a straightforward, but simplified, assumption. To explore the full range of possible initial

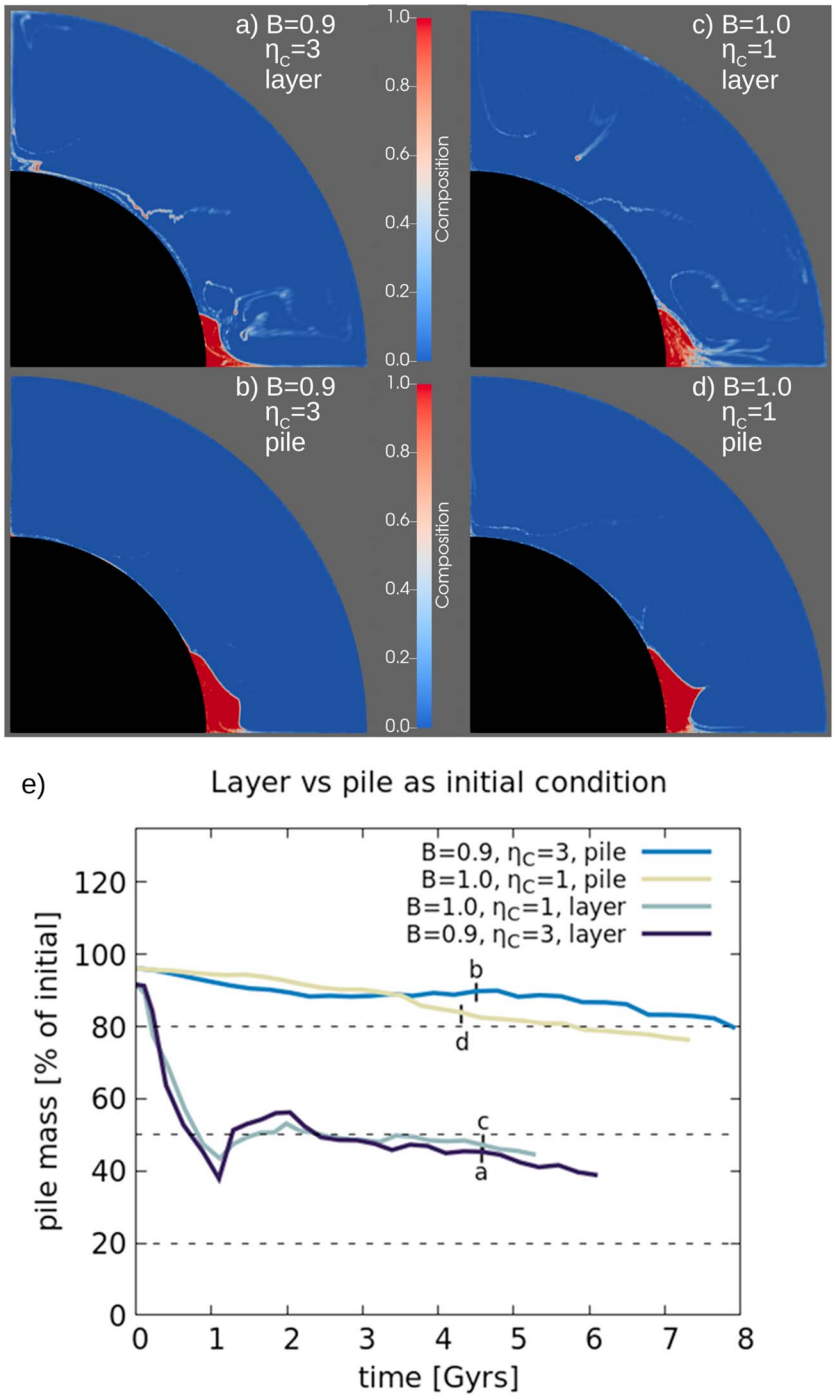

Figure 4. Comparison of compositional structures 4.5 Gyr after starting models with (top row) a dense basal layer and (bottom row) a fully developed pile. (a) and (b) compare results for $B = 0.9$ and $\eta_C = 3$; (c) and (d) compare results for $B = 1.0$ and $\eta_C = 1$; all models use $\eta_{\Delta T} = 65$. (e) Temporal evolution of the pile mass ($cl = 0.8$) for models in (a)–(d). The higher mass at $t = 0$ for the pile models is due to compaction and reduction of surface area during pile formation for $B = 1.2$.

conditions for composition, we also perform simulations in which we start our models with a fully developed pile structure, which we obtain after 5.0 Gyr for $B = 1.2$, $\eta_C = 10$, and $\eta_{\Delta T} = 2.3$. The thermal viscosity contrast is set to $\eta_{\Delta T} = 65$, and we observe a similar trade-off between buoyancy ratio and compositional viscosity contrast as before. However, significantly decreasing either (or even both) B and η_C still results in stable thermochemical piles. As can be seen in Figures 4c and 4d, a buoyancy ratio of $B = 0.9$ for $\eta_C = 3$ or no compositional

viscosity contrast ($\eta_C = 1$) for $B = 1.0$ are sufficient to keep entrainment low, while these combinations of parameters are not suitable to form stable piles if we start with a layer of dense material (Figures 4a and 4b).

If we compare the temporal evolution of the pile mass for models starting with a pile to those that start with a dense basal layer as shown in Figure 4e, the strong influence of deformation-induced entrainment during pile formation becomes apparent. The pile mass for models with preformed structures stays almost constant or decreases only slightly with time, while calculations starting with a dense layer show the characteristic mass loss during the first 1–2 Gyr as discussed above, without permanent recovery. Hence, the requirements for stability depend on the initial configuration of the dense material and temperature, and the observed entrainment during pile formation may result from destruction of the initial temperature gradient. This is because strong deformation, for example, as required to form piles, is accompanied by increased entrainment and mixing between dense material and ambient mantle.

6. Discussion

As already mentioned in section 2, the chosen resolution is not sufficient to resolve details of the entrainment rate, which occurs on length scales <1 km (e.g., Davaille et al., 2002; Jellinek & Manga, 2002). To ensure that our models still qualitatively capture the dynamics of the dense material, we performed tests with different resolutions. The results show a similar behavior, although lower resolution overestimates material loss (cf. Figure S1). A more detailed discussion can be found in the supporting information. In general, our model setup may underestimate the entrainment after pile formation because we assume a stable convection pattern, which might not be true throughout Earth's history. However, tests with reversed plate velocity after pile formation indicate that piles tend to persist if they survive formation with $m > 80\%$ (Figure S2).

Since we force the flow to a degree-2 structure, we cannot fully investigate stability with respect to pile position or spherical harmonic degree. However, piles react to changes in mantle flow, for example, thermal instabilities next to the pile margin. Growing instabilities deflect the pressure that downwellings apply to the pile, allowing the dense material to flatten. When the plume is finally pushed against the edge of the pile, the LLSVP structure is compressed and lifted upward, resulting in steep sides. A lower density contrast or a lower compositional viscosity of the pile amplifies this radial and horizontal movement because the material can react more rapidly.

In our models, we assume primordial material as a source for the LLSVPs, in agreement with, for example, Deschamps et al. (2012). However, subducted MORB accumulating at the CMB may also be a candidate (e.g., Mulyukova et al., 2015), although this process is still under debate (Li & McNamara, 2013). The high bulk modulus of basalt reduces its excess density with depth, which causes almost neutral buoyancy of the material at CMB conditions (Ballmer et al., 2016; Li & McNamara, 2013; Mulyukova et al., 2015). In our models, even intrinsically strong piles require an original excess density of ~1.9% during pile formation, which argues for primordial material. This inferred excess density is larger than estimated by Koelemeijer et al. (2017) and Lau et al. (2017), but most of our piles contain small portions of ambient mantle, which reduces the pile's overall excess density. A similar reduction would be caused by small portions of basalt mixing into the primordial material (Ballmer et al., 2016), but MORB's intrinsic high viscosity would not impact pile viscosity as much (Ballmer et al., 2016). Consequently, we do not expect a significant impact on pile stability for small fractions of basalt mixing into the pile after its formation.

7. Conclusions

Our 2-D calculations indicate a strong impact of compositional viscosity contrasts on the stability of dense pile structures, especially for low thermal viscosity contrasts (e.g., Yang & Gurnis, 2016). In agreement with Davaille et al. (2002), internal viscosity due to composition significantly reduces pile entrainment rates, especially during stages of strong deformation of the dense material. In general, the chemical viscosity contrasts necessary for pile stability decrease with increasing thermal viscosity contrast and/or buoyancy ratio. For our calculations, a limit of stability is reached at about 1.9% excess density ($B = 0.56$), as lower excess density requires considerably higher compositional and/or thermal viscosity contrasts than we used. Requirements for stability are lower if the dense material does not have to survive an initial overturn event. However, if the reaction between mantle and core has been extensive enough to convert the dense component to pure bridgmanite, we may expect a chemical viscosity increase of up to 3 orders of magnitude, which may stabilize piles for even

smaller excess densities. On the other hand, mixing between pile material and ambient mantle or subducted basalt can reduce the effective density during pile formation or deformation.

We find that the requirements for long-term pile stability are determined by the pile's deformation history. For example, long-term stability of LLSVP structures is likely if they survive their initial formation without critical mass loss. However, our results assume spatial stability of the piles. Since strong entrainment of pile material is confined to periods of intense deformation, pile survival following a change from degree-2 to degree-1 structure or vice versa should require higher viscosities or densities than compared to survival beneath an enduring degree-2 structure.

Acknowledgments
Model runtime parameters are listed in the supporting information Tables S1 and S2. This work was partly supported by the Research Council of Norway through its Centres of Excellence funding scheme project 223272 and through The Norwegian Research School DEEP project 249040/F60. Computation time was provided by the Norwegian infrastructure for high-performance computing (Notur) via allocations NN9283K/NS9029K. Thanks to Fabio Crameri, Abigail Bull-Aller, Jeroen Ritsema, Maxim Ballmer, and two anonymous reviewers for valuable input.

References

Austermann, J., Kaye, B. T., Mitrovica, J. X., & Huybers, P. (2014). A statistical analysis of the correlation between large igneous provinces and lower mantle seismic structure. *Geophysical Journal International*, *197*, 1–9. https://doi.org/10.1093/gji/ggt500

Ballmer, M. D., Lourenco, D. L., Hirose, K., Caracas, R., & Nomura, R. (2017). Reconciling magma-ocean crystallization models with the present-day structure of the Earth's mantle. *Geochemistry, Geophysics, Geosystems*, *18*, 2785–2806. https://doi.org/10.1002/2017GC006917

Ballmer, M. D., Schumacher, L., Lekic, V., Thomas, C., & Ito, G. (2016). Compositional layering within the large low shear-velocity provinces in the lower mantle. *Geochemistry, Geophysics, Geosystems*, *17*, 5056–5077. https://doi.org/10.1002/2016GC006605

Bower, D. J., Gurnis, M., & Seton, M. (2013). Lower mantle structure from paleogeographically constrained dynamic Earth models. *Geochemistry, Geophysics, Geosystems*, *14*, 44–63. https://doi.org/10.1029/2012GC004267

Chauvel, C., Maury, R. C., Blais, S., Lewin, E., Guillou, H., Guille, G., et al. (2012). The size of plume heterogeneities constrained by Marquesas isotopic stripes. *Geochemistry, Geophysics, Geosystems*, *13*, Q07005. https://doi.org/10.1029/2012GC004123

Conrad, C. P., Steinberger, B., & Torsvik, T. H. (2013). Stability of active mantle upwelling revealed by net characteristics of plate tectonics. *Nature*, *498*(7455), 479–482. https://doi.org/10.1038/nature12203

Cottar, S., & Lekic, V. (2016). Morphology of seismically slow lower-mantle structures. *Geophysical Journal International*, *207*, 1122–1136. https://doi.org/10.1093/gji/ggw324

Davaille, A., Girard, F., & Le Bars, M. (2002). How to anchor hotspots in a convecting mantle? *Earth and Planetary Science Letters*, *203*, 621–634.

Davies, D. R., Goes, S., & Sambridge, M. (2015). On the relationship between volcanic hotspot locations, the reconstructed eruption sites of large igneous provinces and deep mantle seismic structure. *Earth and Planetary Science Letters*, *411*, 221–130. https://doi.org/10.1016/j.epsl.2014.11.052

Davies, D. R., Goes, S., Schuberth, B. S. A., Bunge, H. P., & Ritsema, J. (2012). Reconciling dynamic and seismic models of Earth's lower mantle: The dominant role of thermal heterogeneity. *Earth and Planetary Science Letters*, *353*, 253–269. https://doi.org/10.1016/j.epsl.2012.08.016

Deschamps, F., Cobden, L., & Tackley, P. J. (2012). The primitive nature of large low shear-wave velocity provinces. *Earth and Planetary Science Letters*, *349–350*, 198–208. https://doi.org/10.1016/j.epsl.2012.07.012

Dziewonski, A. M., Lekic, V., & Romanowicz, B. A. (2010). Mantle anchor structure: An argument for bottom up tectonics. *Earth and Planetary Science Letters*, *299*, 69–79. https://doi.org/10.1016/j.epsl.2010.08.013

Frost, D. J., Asahara, Y., Rubie, D. C., Miyajima, N., Dubrovinsky, L. S., Holzapfel, C., et al. (2010). Partitioning of oxygen between the Earth's mantle and core. *Journal of Geophysical Research*, *115*, B02202. https://doi.org/10.1029/2009JB006302

Garnero, E. J., & McNamara, A. K. (2008). Structure and dynamics of Earth's lower mantle. *Science*, *230*, 626–628.

Garnero, E. J., McNamara, A. K., & Shim, H.-S. (2016). Continent-sized anomalous zones with low seismic velocity at the base of Earth's mantle. *Nature Geoscience*, *9*, 481–489. https://doi.org/10.1038/NGEO2733

Hager, B. H., Clayton, R. W., Richards, M. A., Comer, R. P., & Dziewonski, A. M. (1985). Lower mantle heterogeneity, dynamic topography and the geoid. *Nature*, *313*, 541–545.

Hirose, K., Morard, G., Sinmyo, R., Umemoto, K., Hernlund, J., Helffrich, G., & Labrosse, S. (2017). Crystallization of silicon dioxide and compositional evolution of the earth's core. *Nature*, *543*, 99–102. https://doi.org/10.1038/nature21367

Jellinek, A. M., & Manga, M. (2002). The influence of a chemical boundary layer on the fixity, spacing and lifetime of manlte plumes. *Nature*, *418*, 760–763. https://doi.org/10.1038/nature00979

Koelemeijer, P., Deuss, A., & Ritsema, J. (2017). Density structure of Earth's lowermost mantle from Stoneley mode splitting observations. *Nature Communications*, *8*, 15241. https://doi.org/10.1038/ncomms15241

Labrosse, S., Hernlund, J. W., & Coltice, N. (2007). A crystallizing dense magma ocean at the base of the Earth's mantle. *Nature*, *450*, 866–869.

Lau, H. C. P., Mitrovica, J. X, Davis, J. L., Tromp, J., Yang, H.-Y., & Al-Attar, D. (2017). Tidal tomography constrains Earth's deep-mantle buoyancy. *Nature*, *551*, 321–326. https://doi.org/10.1038/nature24452

Lee, C.-T. A., Luffi, P., Höink, T., Li, J., Dasgupta, R., & Hernlund, J. (2010). Upside-down differentiation and generation of a 'primordial' lower mantle. *Nature*, *463*, 930–933. https://doi.org/10.1038/nature08824

Lekic, V., Cottaar, S., Dziewonski, A., & Romanowicz, B. (2012). Cluster analysis of global lower mantle tomography: A new class of structure and implications for chemical heterogeneity. *Earth and Planetary Science Letters*, *357*, 68–77.

Li, Y., Deschamps, F., & Tackley, P. J. (2014). The stability and structure of primordial reservoirs in the lower mantle: Insights from models of thermochemical convection in three-dimensional spherical geometry. *Geophysical Journal International*, *199*, 914–930. https://doi.org/10.1093/gji/ggu295

Li, Y., Deschamps, F., & Tackley, P. J. (2015). Effects of the post-perovskite phase transition properties on the stability and structure of primordial reservoirs in the lower mantle of the Earth. *Earth and Planetary Science Letters*, *432*, 1–12. https://doi.org/10.1016/j.epsl.2015.09.040

Li, M., & McNamara, A. K. (2013). The difficulty for subducted oceanic crust to accumulate at the Earth's core-mantle boundary. *Journal of Geophysical Research: Solid Earth*, *118*, 1807–1816. https://doi.org/10.1002/jgrb.50156

Li, M., McNamara, A. K., & Garnero, E. J. (2014). Chemical complexity of hotspots caused by cycling oceanic crust through mantle reservoirs. *Nature Geoscience*, *7*, 366–370. https://doi.org/10.1038/NGEO2120

Liu, X., & Zhong, S. (2015). The long-wavelength geoid from three-dimensional spherical models of thermal and thermochemical mantle convection. *Journal of Geophysical Research: Solid Earth*, *120*, 4572–4596. https://doi.org/10.1002/2015JB012016

McNamara, A. K., & Zhong, S. (2004). Thermochemical structures within a spherical mantle: Superplumes or Piles? *Journal of Geophysical Research*, *109*, B07402. https://doi.org/10.1029/2003JB002847

McNamara, A. K., & Zhong, S. (2005). Thermochemical structures beneath Africa and the Pacific Ocean. *Nature*, *437*, 1136–1139. https://doi.org/10.1038/nature04066

Mulyukova, E., Steinberger, B., Dabrowski, M., & Sobolev, S. V. (2015). Survival of LLSVPs for billions of years in a vigorously convecting mantle: Replenishment and destruction of chemical anomaly. *Journal of Geophysical Research: Solid Earth*, *120*, 3824–3847. https://doi.org/10.1002/2014JB011688

Nakagawa, T., & Tackley, P. J. (2011). Effects of low-viscosity post-perovskite on thermo-chemical mantle convection in a 3-D spherical shell. *Geophysical Research Letters*, *38*, L04309. https://doi.org/10.1029/2010GL046494

Schuberth, B. S. A., Bunge, H.-P., & Ritsema, J. (2009). Tomographic filtering of high-resolution mantle circulation models: Can seismic heterogeneity be explained by temperature alone? *Geochemistry, Geophysics, Geosystems*, *10*, Q05W03. https://doi.org/10.1029/2009GC002401

Schuberth, B. S. A., Bunge, H.-P., Steinle-Neumann, G., Moder, C., & Oeser, J. (2009). Thermal versus elastic heterogeneity in high-resolution mantle circulation models with pyrolite composition: High plume excess temperatures in the lowermost mantle. *Geochemistry, Geophysics, Geosystems*, *10*, Q01W01. https://doi.org/10.1029/2008GC002235

Schuberth, B. S. A., Zaroli, C., & Nolet, G. (2012). Synthetic seismograms for a synthetic Earth: Long-period P- and S-wave traveltime variations can be explained by temperature alone. *Geophysical Journal International*, *188*, 1393–1412. https://doi.org/10.1111/j.1365-246X.2011.05333.x

Simmons, N. A., Forte, A. M., & Grand, S. P. (2009). Joint seismic, geodynamic and mineral physical constraints on three-dimensional mantle heterogeneity: Implications for the relative importance of thermal versus compositional heterogeneity. *Geophysical Journal International*, *177*, 1284–1304. https://doi.org/10.1111/j.1365-246X.2009.04133.x

Steinberger, B., & Torsvik, T. H. (2012). A geodynamic model of plumes from the margins of large low shear velocity provinces. *Geochemistry, Geophysics, Geosystems*, *13*, Q01W09. https://doi.org/10.1029/2011gc003808

Tackley, P. J. (2012). Dynamics and evolution of the deep mantle resulting from thermal, chemical, phase and melting effects. *Earth-Science Reviews*, *110*, 1–25. https://doi.org/10.1016/j.earscirev.2011.10.001

Tackley, P. J., & King, S. D. (2003). Testing the tracer ratio method for modeling active compositional fields in mantle convection simulations. *Geochemistry, Geophysics, Geosystems*, *4*(4), 8302. https://doi.org/10.1029/2001GC000214

Tan, E., Choi, E., Thoutireddy, P., Gurnis, M., & Aivazis, M. (2006). GeoFramework: Coupling multiple models of mantle convection within a computational framework. *Geochemistry, Geophysics, Geosystems*, *7*, Q06001. https://doi.org/10.1029/2005GC001155

Torsvik, T. H., Burke, K., Steinberger, B., Webb, S. C., & Ashwal, L. D. (2010). Diamonds sourced by plumes from the core mantle boundary. *Nature*, *466*, 352–355.

Torsvik, T. H., Steinberger, B., Ashwal, L. D., Doubrovine, P. V., & Trønnes, R. G. (2016). Earth evolution and dynamics—A tribute to Kevin Burke. *Canadian Journal of Earth Sciences*, *53*, 1–15. https://doi.org/10.1139/cjes-2015-0228

Torsvik, T. H., van der Voo, R., Doubrovine, P. V., Burke, K., Steinberger, B., et al. (2014). Deep mantle structure as a reference frame for movements in and on the Earth. *Proceedings of the National Academy of Sciences*, *111*(24), 8735–8740. https://doi.org/10.1073/pnas.1318135111

Yang, T., & Gurnis, M. (2016). Dynamic topography, gravity and the role of lateral viscosity variations from inversion of global mantle flow. *Geophysical Journal International*, *207*, 1186–1202. https://doi.org/10.1093/gji/ggw335

Zhong, S., Zuber, M. T., Moresi, L. N., & Gurnis, M. (2000). The role of temperature-dependent viscosity and surface plates in spherical shell models of mantle convection. *Journal of Geophysical Research*, *105*, 11,063–11,082.